Antoñanzas, C.; Ferrer Contreras, M.; De Diego Antón, M.; Gonzalez, A. (2023). Remote Microphone Technique for Active Noise Control Over Distributed Networks. IEEE/ACM Transactions on Audio Speech and Language Processing. 31:1522-1535. https://doi.org/10.1109/TASLP.2023.3264600

# Remote microphone technique for active noise control over distributed networks

Christian Antoñanzas, Miguel Ferrer, *Member, IEEE*, Maria de Diego, *Senior Member, IEEE*, Alberto Gonzalez, *Senior Member, IEEE*

***Abstract*—Multichannel Active Noise Control (ANC) headrest systems have usually been designed with the objective of creating quiet areas at the passenger positions within the cabin of a public transport. Due to the high computational demands of dealing with multiple loudspeakers and multiple microphones by using a single centralized processor, and the convenience of a scalable system, a distributed implementation may be advisable. On the other hand, the addition of the remote microphone (RM) technique to the ANC headrest systems has recently allowed the creation of local zones of quiet at unachievable placements for the error sensors. This technique allows the quiet zone to be shifted to a desired location away from the physical sensor. However, to our knowledge, the implementation of an ANC headrest system with virtual microphones over a distributed acoustic sensor network has not been addressed. In this work, a distributed version of the multiple-error FxLMS (MEFxLMS) algorithm considering the RM method (RM-DMEFxLMS) is proposed by using an alternative formulation of the RM method. Through a set of simulations, it is found that on a non-constrained communication network, the proposed algorithm presents the same performance of its centralized version and provides a scalable and more versatile ANC system.**

***Index Terms*—Remote microphone, active noise control, distributed processing, acoustic sensor networks.**

## I. Introduction

ACTIVE Noise Control (ANC) headrest systems have been developed to reduce the sound level of undesired noise in the listener's ears, avoiding active headphones [1]–[3]. Generally, several actuators are placed near the headrest to generate the anti-noise signals, while several sensors located close to the listener's ears pick up the error signals. Depending on the control strategy, a reference microphone signal (feedforward control) [4], [5] or an internally estimated signal (feedback control) [6], [7] are used to obtain a reference signal that is correlated to the undesired noise. It is also worth noting that deep learning techniques have been recently applied to ANC problems [8]–[10]. The resulting quiet zones around the error sensors are generally limited in size and remain approximately within a sphere whose diameter is one tenth of the wavelength of the highest frequency of the noise [11], [12]. The noise level may even increase away from these zones [13]. This requires the error sensors be located as close as possible to the listener's ears, which is often uncomfortable. Thus, the remote microphone (RM) [14] and virtual sensing [15] techniques are effective methods for projecting a quiet zone to the desired position and have attracted increasing attention in recent years. Several authors have proposed ANC systems based on the RM method [16]–[21] to achieve noise cancellation at a target position (virtual location) where the microphones cannot be located. To this end, the control system minimizes the signals that the virtual sensors would pick up, but it uses the signals captured by a set of physical sensors, called monitoring sensors, that are located away from the quiet zone. By using several previously calculated *observation* functions, the RM technique is able to estimate the primary disturbance at the virtual sensors from the primary disturbance measured at the monitoring sensors. That allows us to directly estimate the error signals at the virtual sensors from the error signals at the monitoring sensors. It should be noted that the stability of these ANC systems must also be assured when the RM technique is applied. Since the stability can be compromised due to inherent uncertainties related to the control of the sound field [22]. Therefore, new schemes have recently been proposed to improve the performance and robustness of the ANC systems [23]–[25].

On the other hand, ANC headrest systems attempt to create noise-free zones at all listener locations in a listening area or room. That involves multiple loudspeakers and microphones that are linked to the same centralized processor, which picks up, processes, and generates multiple signals. However, the computational burden of a single controller may increase significantly due to the use of multiple transducers and overflowing its capacity. On the contrary, a distributed approach can divide this computation between several processors. Furthermore ANC systems may usually require a change in the number or positions of transducers. In such cases, a distributed approach is often preferred since it provides independent processing and control. Therefore, the use of distributed ANC systems eliminates dependence on the capacity of a single central system, making the ANC systems more versatile and scalable. In addition, the acoustic interaction between loudspeakers and microphones must also be taken into consideration in the multichannel distributed ANC system [26], [27]. In cases where such interaction does not significantly affect the sys-

Christian Antoñanzas is with the Universidad Internacional de La Rioja (UNIR), 26002 Logroño, Spain (e-mail: cristian.antonanzas@unir.net).

Miguel Ferrer, Maria de Diego and Alberto Gonzalez are with the Institute of Telecommunications and Multimedia Applications (iTEAM), Universitat Politècnica de València (UPV), 46022 Valencia, Spain (e-mail: mferrer@dcom.upv.es; mdediego@dcom.upv.es; agonzal@dcom.upv.es).

This work has been partially supported by RTI2018-098085-BC41 and PID2021-125736OB-I00 (MCIN/AEI/10.13039/501100011033/, "ERDF A way of making Europe") and GVA through PROMETEO/2019/109.

Manuscript received xxx xx, 2022; revised xxx xx, 2022.

tem´s performance (e.g., if loudspeakers and microphones of different subsystems are sufficiently separated), it is possible to achieve global system stability by using independent and non-collaborative processing systems. That results in a decentralized approach [27]–[29]. Nevertheless, acoustic coupling among transducers is present in most practical cases and could also lead to an impairment of the behavior and stability of the ANC system in many cases [30]. Therefore, the use of collaborative algorithms for distributed multichannel ANC systems must be considered. This collaboration takes into account the effects of the acoustical interaction and ensures global system stability while providing cancellation performance similar to the centralized approach. A distributed version of the Multiple Error FxLMS (MEFxLMS) algorithm [26] was presented in [31] and named DMEFxLMS. This work considers a distributed ANC system composed of autonomous acoustic nodes that are capable of measuring and generating signals to reach a noise control target using a homogeneous acoustic sensor network (ASN) [32]. ASNs are specifically designed for acoustic signal processing tasks and are a popular and efficient solution for different applications in multiple acoustic areas such as: environmental audio monitoring [33], sound source location [34], [35], speech enhancement [36], blind synchronization [37], and binaural hearing aids [38], among others. The ASN introduced in [31] is a ring-topology sensor network that is composed of acoustic single-channel nodes, which are equipped with a single sensor and a single actuator, share the same communications and computation capacities, and execute the DMEFxLMS algorithm. As presented in [31], a collaborative ASN with ring topology based on incremental communication among the nodes [39] could obtain the same performance as its corresponding centralized algorithm. Thus, to improve the implementation of this algorithm in practical scenarios, several collaborative distributed approaches have been proposed taking into account implementation aspects such as convergence rate [40], [41], hardware constraints [42], and efficient performance [43].

To our knowledge, the implementation of ANC headrest systems using the RM technique over ASNs has not yet been developed. Accordingly, one of the main objectives of this work is to apply the RM technique to distributed systems by reviewing the centralized formulation presented in [44] and proposing a distributed approach. More specifically, we present a distributed ANC headrest system based on the MEFxLMS algorithm combined with the RM technique over ASNs based on incremental communication among the nodes. We denote this strategy as the RM-DMEFxLMS algorithm, which should provide the same performance as the centralized version (which we refer to as the RM-MEFxLMS algorithm) under good communication conditions. In the proposed RM-DMEFxLMS algorithm, each node uses a local version of the global adaptive filter, which is updated and exchanged among the nodes following incremental learning. The performance of the new distributed approach based on virtual sensors compared to its centralized version over a homogeneous ASN is evaluated. An analysis of implementation considerations, such as the computational complexity and the communication demands, is also presented. Since each node can independently compute a part of the global adaptive filter, the presented algorithm can be used in heterogeneous networks and the distributed scheme can be adapted to work with other network topologies and data sharing strategies.

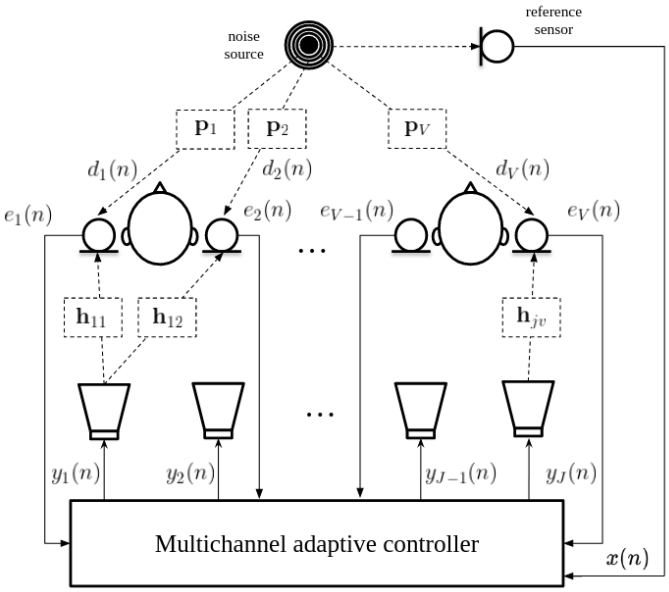


Fig. 1. Multichannel centralized ANC headrest system.

The paper is organized as follows: In Section II, we formulate the multichannel ANC system based on the centralized MEFxLMS algorithm and the ANC system based on the RM technique (RM-MEFxLMS). This section also introduces the distributed version of the RM-MEFxLMS, leading to the RM-DMEFxLMS over ASNs based on incremental learning. Section III studies the performance of the RM-DMEFxLMS algorithm for an ANC headrest system compared to the MEFxLMS and the RM-MEFxLMS algorithms. Finally, Section IV outlines the main conclusions of the present work.

*Notation*: For the sake of clarity, the following notation has been used throughout this work: italics denote scalars (e.g., $x$), boldface lower-case letters denote vectors (e.g., $\mathbf{x}$), and boldface upper-case letters denote matrices (e.g., $\mathbf{X}$). Boldface subindexes denote type of sensor (e.g., $e_{\mathbf{m}}$ refers to a scalar related to the monitoring sensor). The character ˜ indicates an estimation of the given signal or system.

## II. Description of the Algorithms

Let us consider a multichannel centralized ANC headrest system based on the FxLMS algorithm [45] and composed of $J$ actuators and $V$ sensors, as shown in Fig. 1. The single ANC controller receives the information picked up by all of the sensors and aims to control the sound field by generating control signals via all of the actuators. The objective is to cancel the acoustic noise signal at each sensor location, $d_v(n)$ (where $v \in \{1, \ldots, V\}$). Adaptive techniques combined with the filtered-x structure are usually considered in the estimation of the control signals [46]. To this end, the control signal $y_j(n)$ (where $j \in \{1, \ldots, J\}$), which is rendered by the $j$-th actuator and propagated through the acoustic system, is

TABLE I
NOTATION FOR THE RM-MEFXLMS ALGORITHMS

| Notation | Definition |
|---|---|
| $x(n)$ | reference signal. We consider one disturbance noise. |
| $y_j(n)$ | control signal at the $j$-th actuator. |
| $e_{\mathbf{m},k}(n)$ | error signal at the $k$-th monitoring sensor. |
| $e_v(n)$ | error signal at the $v$-th virtual sensor. |
| $d_{\mathbf{m},k}(n)$ | acoustic noise signal at the $k$-th monitoring sensor. |
| $d_v(n)$ | acoustic noise signal at the $v$-th virtual sensor. |
| $\mathbf{w}_j(n)$ | adaptive filter coefficients at the $j$-th actuator. |
| $\mathbf{h}_{\mathbf{m},jk}$, $\mathbf{h}_{jv}$ | acoustic channels that link the $j$-th actuator with the $k$-th monitoring sensor and the $v$-th virtual sensor, respectively. |
| $\mathbf{o}_{kv}$ | observation filters that link the $k$-th monitoring sensor with the $v$-th virtual sensor. |
| $J$ | number of actuators. |
| $K$ | number of monitoring sensors. |
| $V$ | number of virtual sensors. |
| $L$ | number of coefficients of each adaptive filter. |
| $M$ | number of coefficients of the estimated acoustic channels. |
| $P$ | number of coefficients of the observation filters. |
| $Q$ | number of acoustic nodes. |

designed to minimize the signal recorded at $v$-th sensor, called error signal, and denoted by $e_v(n)$ (where $v\in\{1,\dots,V\}$). The application of the filtered-x scheme in the adaptive algorithm requires the estimation of the secondary path channels, $h_{jv}(n)$, that link the $j$-th actuator and the $v$-th sensor. Those acoustic channels are usually modelled as FIR filters of $M$ coefficients, denoted as $\tilde{\mathbf{h}}_{jv}$. It is common to assume ideal path estimation (e.g., $\tilde{\mathbf{h}}_{jv}=\mathbf{h}_{jv}$). The acoustic noise signal at the $v$-th sensor, $d_v(n)$, is modeled as the noise signal filtered through the acoustic (primary) channel between the noise source and the $v$-th sensor, denoted as $p_v(n)$. We assume that $x(n)$ is the reference signal at the discrete time instant $n$ picked up by a reference sensor.

The vector $\mathbf{w}_j(n)$ holds the $L$ coefficients of the FIR filter of the $j$-th actuator. As demonstrated in [26], the vector $\mathbf{w}_j(n)$ minimizes the summation of the instantaneous square of the noise signals at the sensors and it is updated by

$$\mathbf{w}_j(n) = \mathbf{w}_j(n-1) \; -2\mu \sum_{v=1}^{V} \mathbf{u}_{jv} e_v(n), \tag{1}$$

where $\mu$ is the step-size parameter and $\mathbf{u}_{jv}(n)=\mathbf{X}(n)\tilde{\mathbf{h}}_{jv}$, with $\mathbf{X}(n)$ being a matrix of size $[L\times M]$ defined as $\mathbf{X}(n)=[\mathbf{x}(n)\ \mathbf{x}(n-1)\ \dots\ \mathbf{x}(n-M+1)]$, with $\mathbf{x}(n)$ as a $[L\times 1]$ vector holding the most recent $L$ samples of $x(n)$. The output signal of the $j$-th actuator is thus given by

$$y_j(n) = \mathbf{w}_j^T(n)\mathbf{x}(n), \tag{2}$$

and the error signal at the $v$-th sensor can be expressed as

$$e_v(n) = d_v(n) + \sum_{j=1}^{J} h_{jv}(n) * y_j(n), \tag{3}$$

with $*$ denoting the linear convolution operator. Note that (1) is the updating equation for the $j$-th adaptive filter of the MEFxLMS algorithm. However, although significant attenuation can be achieved at each error sensor location, the quiet zones are usually small since they are inversely proportional to the maximum frequency of the noise signal. Consequently, it is necessary to place the error sensors as close as possible to the listener's ears, which is often a drawback. To overcome these problems, the remote microphone technique has been developed to shift the quiet zone away from the physical position of the sensor to another desired location. On this basis, the centralized version of the MEFxLMS algorithm considering the remote microphone method (RM-MEFxLMS) is briefly described in Section II-B. First, the observation filters that link the primary disturbance measured at the monitoring sensors with the virtual sensors are modelled in a setup phase.

### A. Estimation of noise signals by observation filters

Fig. 2 illustrates the block diagram of a multichannel centralized ANC system using the remote microphone method. In the following, $J$ actuators, $K$ monitoring sensors, and $V$ virtual sensors are considered. The aim is to cancel the acoustic noise signal at the virtual sensor locations, $d_v(n)$ $\forall v$. Since the actual signals at the virtual sensors cannot be directly measured, the remote microphone technique considers that the virtual sensor signals can be estimated from the signals picked up at a set of $K$ monitoring sensors. This is achieved through the use of the corresponding observation functions, which are usually estimated in a previous stage by means of $P$-order FIR filters. A given observation function relates the noise signal at a virtual control point, $d_v(n)$, with the noise signal measured at the positions where the monitoring sensors are located, $d_{\mathbf{m},k}(n)$ with $k\in\{1,\dots,K\}$. It is important to note that the robustness of the ANC system depends on the choice of the proper modelling order, $P$, as well as the number and location of the monitoring microphones [44]. The noise signal picked up at the $v$-th virtual sensor can be estimated as

$$\tilde{d_v}(n) = \sum_{k=1}^{K} o_{kv}(n) * d_{\mathbf{m},k}(n), \tag{4}$$

where $o_{kv}(n)$ denotes the observation filter that links the $k$-th monitoring sensor with the $v$-th virtual sensor. At a setup stage, physical microphones are placed on the targets (virtual microphone positions) to estimate the observation filters. Note that, when the algorithm is working, the microphones placed at the virtual control points will not be available. Because of this, the observation filters should be previously calculated using

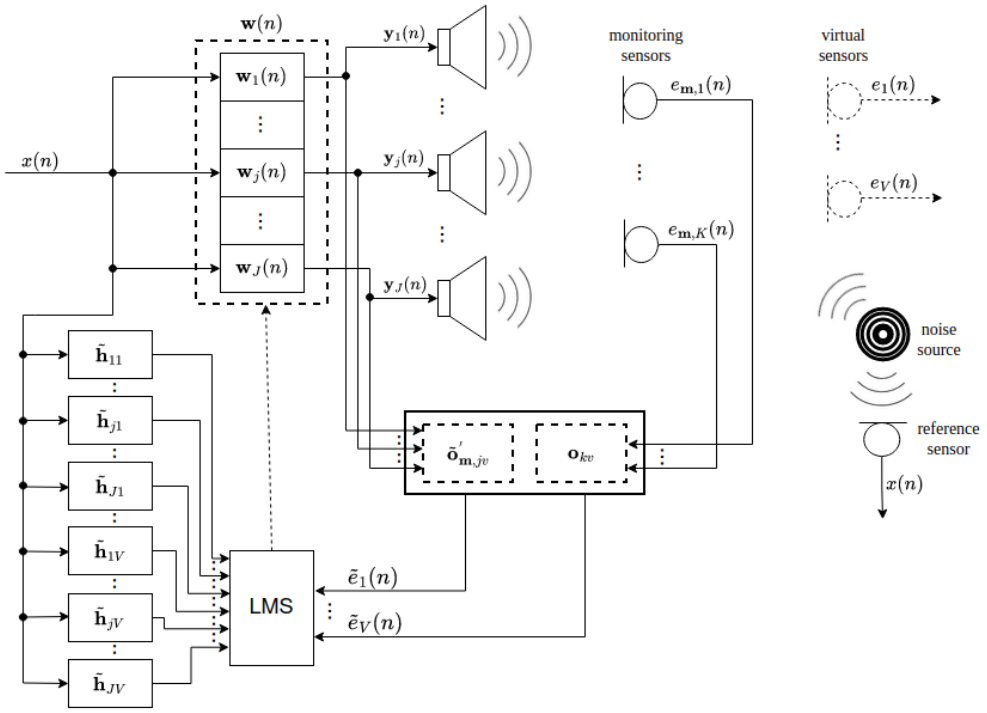


Fig. 2. Block diagram of a multichannel centralized ANC system using the remote microphone technique. The box, which contains the $\tilde{\mathbf{o}}'_{\mathbf{m},jv}$ and $\mathbf{o}_{kv}$ observation filters, performs the calculation described by (7).

suitably selected measurements. This method is summarized in Appendix A.

With regard to the calculation of the observation filters, a more detailed explanation can be found in [18], [19], [44]. However, some aspects must be considered. The relative physical positions among virtual and monitoring microphones significantly influence the performance of the RM algorithms. In other words, the shapes of the quiet zones around the virtual microphones depend on the location of the monitoring microphones, as demonstrated in [18]. Consequently, given multiple virtual and monitoring sensors, the proper modelling of the observation filters and the relative positions of the sensors will improve the algorithm behavior. Thus, an experimental study on the best positioning of the monitoring sensors in a practical acoustic environment is included in the results presented in Section III, with the aim of illustrating a suitable estimation of the signals at the virtual points from the signals at the monitoring sensors.

### *B. The RM-MEFxLMS algorithm*

We can approximate the behavior of the algorithm described by (1) and (2) by estimating the virtual sensor error signals from the actual error signals picked up at the monitoring sensors, and thus we can develop an algorithm for practical use. The primary disturbance signals at the monitoring sensors can be estimated from the actual error signals as:

$$\tilde{d}_{\mathbf{m},k}(n) = e_{\mathbf{m},k}(n) - \sum_{j=1}^{J} \tilde{h}_{\mathbf{m},jk}(n) * y_j(n), \qquad (5)$$

where $\tilde{h}_{\mathbf{m},jk}(n)$ is the measured acoustic channel between the $j$-th actuator and the $k$-th monitoring sensor, and $e_{\mathbf{m},k}(n)$ is the error signal at the $k$-th monitoring sensor. From the assumptions in Section II-A and considering (5) to be accurate enough, (4) can be expressed as

$$\tilde{d}_v(n) = \sum_{k=1}^{K} o_{kv}(n) * e_{\mathbf{m},k}(n) - \sum_{j=1}^{J} \tilde{o}_{\mathbf{m},jv}(n) * y_j(n), \quad (6)$$

being $\tilde{o}_{\mathbf{m},jv}(n) = \sum_{k=1}^{K} o_{kv}(n) * \tilde{h}_{\mathbf{m},jk}(n)$. The error signals at the virtual points, $\tilde{e}_v(n)$, are estimated according to (3) and (6), leading to

$$\tilde{e}_v(n) = \sum_{k=1}^{K} o_{kv}(n) * e_{\mathbf{m},k}(n) - \sum_{j=1}^{J} \tilde{o}'_{\mathbf{m},jv}(n) * y_j(n), \quad (7)$$

being $\tilde{o}'_{\mathbf{m},jv}(n) = \tilde{o}_{\mathbf{m},jv}(n) - \tilde{h}_{jv}(n)$.

Furthermore the steps to calculate the updated filter coefficients at the $j$-th actuator are described as follows:

1) The error signal $e_{\mathbf{m},k}(n)$ is acquired from the $k$-th monitoring sensor.
2) The estimated error signals at the $v$-th virtual sensor are calculated through (7) using the error signals at the monitoring sensors and the signals generated by the actuators.
3) The filter coefficients at the $j$-th actuator are updated as:

$$\mathbf{w}_j(n) = \mathbf{w}_j(n-1) - 2\mu \sum_{v=1}^{V} \mathbf{u}_{jv} \tilde{e}_v(n). \qquad (8)$$

Table I gathers the notation required for the remote microphone technique applied to ANC. The algorithm steps are described in Algorithm 1. Note that, in practical systems, the error signals are correlated with both the adaptive filter output

**Algorithm 1:** RM-MEFxLMS algorithm

1 *Setup stage*: Calculation of $\tilde{\mathbf{o}}'_{\mathbf{m},jv}, \mathbf{o}_{kv}, \tilde{\mathbf{h}}_{\mathbf{m},jk}$ and $\tilde{\mathbf{h}}_{jv}\ \forall j,k,v$
2 Initialize: $\mathbf{w}_j(0) = [0,\ldots,0]^T\ \forall j$
3 **for** ***all*** $n \geq 0$ **do**
4  Obtain $x(n)$ from the reference sensor
5  $\mathbf{x}(n) = [x(n)\ x(n-1)\ \ldots\ x(n-L+1)]^T$
6  $\mathbf{X}(n) = [\mathbf{x}(n)\ \mathbf{x}(n-1)\ \ldots\ \mathbf{x}(n-M+1)]$
7  **for** ***all*** *monitoring sensor* $1 \leq k \leq K$ **do**
8  Obtain $e_{\mathbf{m},k}(n)$ from the $k$-th monitoring sensor
9  $\mathbf{e}_{\mathbf{m},k}(n) = [e_{\mathbf{m},k}(n)\ e_{\mathbf{m},k}(n-1)\ \ldots\ e_{\mathbf{m},k}(n-P-1)]^T$
10  **end for**
11  **for** ***all*** *actuator* $1 \leq\ j \leq J$ **do**
12  $y_j(n) = \mathbf{w}_j^T(n)\mathbf{x}(n)$ // $L$ Mult.
13  $\mathbf{y}_j(n) = [y_j(n)\ y_j(n-1)\ \ldots\ y_j(n-M-P)]^T$
14  **end for**
15  **for** ***all*** *virtual sensor* $1 \leq\ v \leq V$ **do**
16  $\tilde{e}_v(n) = \sum_{k=1}^{K} \mathbf{o}_{kv}^T \mathbf{e}_{\mathbf{m},k}(n) - \sum_{j=1}^{J} (\tilde{\mathbf{o}}'_{\mathbf{m},jv})^T \mathbf{y}_j(n-1)$ // $PK + J(P+M-1)$ Mult.
17  **end for**
18  **for** ***all*** *actuator* $1 \leq\ j \leq J$ **do**
19  **for** ***all*** *virtual sensor* $1 \leq\ v \leq V$ **do**
20  $\mathbf{u}_{jv}(n) = \mathbf{X}(n)\tilde{\mathbf{h}}_{jv}$ // $M$ Mult.
21  **end for**
22  $\mathbf{w}_j(n+1) = \mathbf{w}_j(n) - 2\mu \sum_{v=1}^{V} \mathbf{u}_{jv}(n-1)\tilde{e}_v(n)$ // $V(L+1)$ Mult.
23  **end for**
24 **end for**

signals and the filtered reference signals. For this reason, a delay of one sample is applied to $\mathbf{u}_{jv}$ and $\mathbf{y}_j$ in the algorithm description. The number of multiplications required for each operation is also shown in Algorithm 1. It is important to observe that the matrix-vector product of line 20 requires only $M$ multiplications, since only one new element of the output vector has to be calculated. Consequently, and as demonstrated in [44], it is possible to derive the updating equation of the global filter of the centralized RM-MEFxLMS algorithm, which is stated as follows:

$$\mathbf{w}(n) = \mathbf{w}(n-1)\ - 2\mu \sum_{v=1}^{V}\ \mathbf{u}_v(n)\tilde{e}_v(n), \tag{9}$$

where $\mathbf{w}(n)$ is the global adaptive filter vector of size $[LJ\times 1]$, which concatenates all of the adaptive filter vectors of each actuator, $\mathbf{w}(n)=[\mathbf{w}_1^T(n)\ \mathbf{w}_2^T(n)\ \ldots\ \mathbf{w}_J^T(n)]^T$. The $[LJ\times 1]$ vector $\mathbf{u}_v(n)$ is defined as $\mathbf{u}_v(n)=[\mathbf{u}_{1v}^T\ \mathbf{u}_{2v}^T\ \ldots\ \mathbf{u}_{Jv}^T]^T$.

Therefore, the centralized algorithm proposed is suitable for multichannel ANC headrest systems based on a single controller to manage all of the signals generated by the actuators and captured by the sensors. However, multichannel systems deployed over a wide area require long communication wiring among the transducers and the controller. That increases the amount of cabling and, consequently, requires more costly infrastructure. Moreover, adding multiple transducers may drastically increase the computational cost needed to capture, manage, and generate multiple signals. It should also not be forgotten that a single controller failure means no information is processed. Then, as stated previously, a distributed approach provides independent processing and control, which is often preferred, especially regarding the flexibility, versatility, and scalability of the system. Hence, the proposed implementation of (9) over a collaborative network of distributed acoustic nodes is presented in Section II-C. This approach aims to have the same behavior of the centralized one under the assumption of ideal network communications, as shown in [31] for the MEFxLMS algorithm.

### *C. The distributed RM-MEFxLMS algorithm*

Let us now consider a multichannel feedforward ANC system that is combined with the remote microphone technique working over a homogeneous ASN of $Q$ nodes, which are spatially distributed within a certain area. A simplified case with $J{=}V{=}Q$ is shown in Fig. 3. A communication network is available to allow data exchange among the nodes. An ideal network with no communication constraints is assumed, where all of the nodes execute the same algorithm and have access to the same reference noise signal, $x(n)$. Every node should be able to locally process its signals and parameters and the information received from its neighbors in order to address the ANC problem, which aims at canceling disturbance noise at the virtual sensor position. In the distributed case, we consider that the $q$-th node is composed of $\{J_q\}$ actuators and $\{K_q\}$ monitoring sensors. Thus, each node is linked to a single set of monitoring sensors and one set of actuators. Since the nodes cannot share any actuator, $\sum_{q=1}^{Q} J_q{=}J$ always holds. If the nodes do not share any monitoring sensor, which usually occurs in practical cases, $\sum_{q=1}^{Q} K_j{=}K$. In addition, we consider that both the observation filters and all of the estimated acoustic channels ($\tilde{\mathbf{h}}_{\mathbf{m},jk}$ and $\tilde{\mathbf{h}}_{jv}$ for all values of $j$, $k$ and $v$) have been calculated in a setup stage and are known before the algorithm starts working.

It is assumed that only the $\{K_q\}$ error signals picked up at the monitoring sensors linked to the $q$-th node are available. Thus, the error signals at the virtual points from (7) can be denoted by the following expression

$$\begin{aligned}\tilde{e}_v(n) = \ & \sum_{q=1}^{Q} \sum_{\forall k\in\{K_q\}} o_{kv}(n) * e_{\mathbf{m},k}(n) \\ & - \sum_{q=1}^{Q} \sum_{\forall j\in\{J_q\}} \tilde{o}'_{\mathbf{m},jv}(n) * y_j(n).\end{aligned} \tag{10}$$

We define $\tilde{e}_{vq}(n)$ as

$$\begin{aligned}\tilde{e}_{vq}(n) \ & = \sum_{\forall k\in\{K_q\}} o_{kv}(n) * e_{\mathbf{m},k}(n) \\ & - \sum_{\forall j\in\{J_q\}} \tilde{o}'_{\mathbf{m},jv}(n) * y_j(n),\end{aligned} \tag{11}$$

where $\tilde{e}_{vq}(n)$ denotes the contribution to the $v$-th error signal that the $q$-th node can independently calculate using its available data, without data exchange among nodes. Therefore, each virtual error can be calculated by the summation of these contributions as:

$$\tilde{e}_v(n) = \sum_{q=1}^{Q} \tilde{e}_{vq}(n). \tag{12}$$

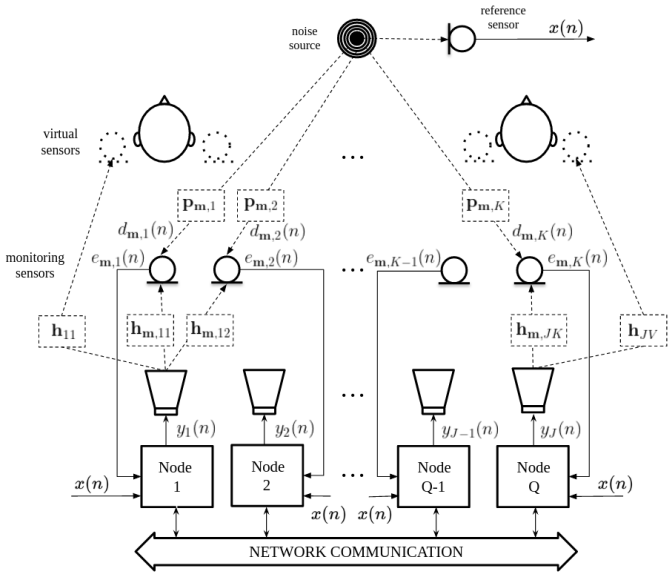


Fig. 3. ASN of $Q$ nodes for an ANC system with the remote microphone technique; in this figure, $J = K = Q$ for simplicity.

Note that the driving signals that belong to other nodes influence the monitoring signal of a certain node, but they are subtracted by the summation over the $\tilde{e}_{vq}(n)$ signals for all the nodes expressed by (12). The adaptive algorithm recursion given by (9) can be formulated using (12) as

$$\begin{aligned}\mathbf{w}(n) &= \mathbf{w}(n-1) - 2\mu \textstyle\sum_{v=1}^{V} \mathbf{u}_v(n) \sum_{q=1}^{Q} \tilde{e}_{vq}(n) \\ &= \mathbf{w}(n-1) - \textstyle\sum_{q=1}^{Q} \left(2\mu \sum_{v=1}^{V} \mathbf{u}_v(n)\tilde{e}_{vq}(n)\right) \\ &= \mathbf{w}(n-1) - \textstyle\sum_{q=1}^{Q} \boldsymbol{\Delta}\mathbf{w}_q(n),\end{aligned} \tag{13}$$

where the term $\boldsymbol{\Delta}\mathbf{w}_q$ can be calculated by the $q$-th node using only its corresponding monitoring error and output signals as well as the parameters estimated during the setup phase. Now, the adaptive processing can be carried out in a distributed way, for example over a ring topology with incremental communication between the nodes, where the global filter $\mathbf{w}(n)$ is split into local updates, as described in [31]. Considering $\mathbf{w}^q(n)$ as a local version of $\mathbf{w}(n)$ at the $q$-th node, from (13), we can derive the filter updating equation of the RM-DMEFxLMS algorithm.

$$\mathbf{w}^q(n) = \mathbf{w}^{q-1}(n) - \boldsymbol{\Delta}\mathbf{w}_q(n), \tag{14}$$

with $q \in \{1, \ldots, Q\}$, where $\mathbf{w}(n) = \mathbf{w}^Q(n)$ at the last node of the ring and $\mathbf{w}^0(n+1) = \mathbf{w}^Q(n)$ at the first node for the next round. A summary of the RM-DMEFxLMS algorithm pseudocode executed per sample time at each node is given in Algorithm 2. Note that an extra data transfer time is required in order to disseminate $\mathbf{w}^Q(n)$ throughout the network. The data transfers and computations carried out at each node using (14) are illustrated by Fig. 4.

To clarify the operations performed by each node both sequentially and in parallel, Fig. 5 shows the time diagram of Algorithm 2 of an ASN composed of Q nodes at the $n$-th iteration. The delay introduced by each process is depicted by the following colors: blue represents the processing delay due to the operations performed by a node with its local information; red shows the delay introduced in the update procedure of $\mathbf{w}^q(n)$ since node $q$ requires the local update

**Algorithm 2:** Distributed RM-MEFxLMS algorithm.

*Setup stage*: Calculation of $\tilde{\mathbf{o}}'_{\mathbf{m},jv}, \mathbf{o}_{kv}, \tilde{\mathbf{h}}_{\mathbf{m},jk}$ and $\tilde{\mathbf{h}}_{jv}$ $\forall j, k, v$
Initialize: $\mathbf{w}^{(0)}(0) = [0, \ldots, 0]^T$
**for *all*** $n \geq 0$ **do**
  **do in parallel**
    Obtain $x(n)$ from the reference sensor
    $\mathbf{x}(n) = [x(n)\ x(n-1)\ \ldots\ x(n-L+1)]^T$
    $\mathbf{X}(n) = [\mathbf{x}(n)\ \mathbf{x}(n-1)\ \ldots\ \mathbf{x}(n-M+1)]$
    **for *all*** *monitoring sensor* $k \in \{K_q\}$ **do**
      Obtain $e_{\mathbf{m},k}(n)$ from the $k$-th monitoring sensor
      $\mathbf{e}_{\mathbf{m},k}(n) = [e_{\mathbf{m},k}(n)\ e_{\mathbf{m},k}(n-1)\ \ldots\ e_{\mathbf{m},k}(n-P-1)]^T$
    **end for**
    **for *all*** *actuator* $j \in \{J_q\}$ **do**
      $\mathbf{w}_j^q(n) = \mathbf{w}^q(n)_{[1+L(j-1):jL]}$
      $y_j(n) = \mathbf{x}^T(n)\mathbf{w}_j^q(n)$ `// L Mult.`
      $\mathbf{y}_j(n) = [y_j(n)\ y_j(n-1)\ \ldots\ y_j(n-M-P)]^T$
    **end for**
    $\boldsymbol{\Delta}\mathbf{w}_q(n) = 0$
    **for *all*** *virtual sensor* $1 \leq v \leq V$ **do**
      $\tilde{e}_{vq}(n) = 0$
      **for *all*** *actuator* $1 \leq j \leq J$ **do**
        $\mathbf{u}_{jv}(n) = \mathbf{X}(n)\tilde{\mathbf{h}}_{jv}$ `// M Mult.`
      **end for**
      $\mathbf{u}_v(n) = [\mathbf{u}_{1v}^T(n)\ \mathbf{u}_{2v}^T(n)\ \ldots\ \mathbf{u}_{Jv}^T(n)]^T$,
      **for *all*** *actuator* $j \in \{J_q\}$ **do**
        $\tilde{e}_{vq}(n) = \tilde{e}_{vq}(n) - (\tilde{\mathbf{o}}'_{\mathbf{m},jv})^T\mathbf{y}_j(n-1)$ `// M + P − 1 Mult.`
      **end for**
      **for *all*** *monitoring sensor* $k \in \{K_q\}$ **do**
        $\tilde{e}_{vq}(n) = \tilde{e}_{vq}(n) + \mathbf{o}_{kv}^T\mathbf{e}_{\mathbf{m},k}(n)$ `// P Mult.`
      **end for**
      $\boldsymbol{\Delta}\mathbf{w}_q(n) = \boldsymbol{\Delta}\mathbf{w}_q(n) + 2\mu\mathbf{u}_v(n-1)\tilde{e}_{vq}(n)$ `// LJ + 1 Mult.`
    **end for**
  **end**
  Calculate: $\mathbf{w}^Q(n)$ ($\mathbf{w}^0(n) \equiv \mathbf{w}^Q(n-1)$).
  **for *all*** *node* $1 \leq q \leq Q$ **do**
    $\mathbf{w}^q(n) \leftarrow \mathbf{w}^{q-1}(n)$ `/* Communication */`
    $\mathbf{w}^q(n) = \mathbf{w}^q(n) - \boldsymbol{\Delta}\mathbf{w}_q(n)$
  **end for**
  Disseminate: $\mathbf{w}^Q(n)$ ($\mathbf{w}^0(n+1) \equiv \mathbf{w}^Q(n)$).
  **for *all*** *node* $1 \leq q \leq Q-1$ **do**
    $\mathbf{w}^q(n+1) \leftarrow \mathbf{w}^{q-1}(n+1)$ `/* Communication */`
  **end for**
**end for**

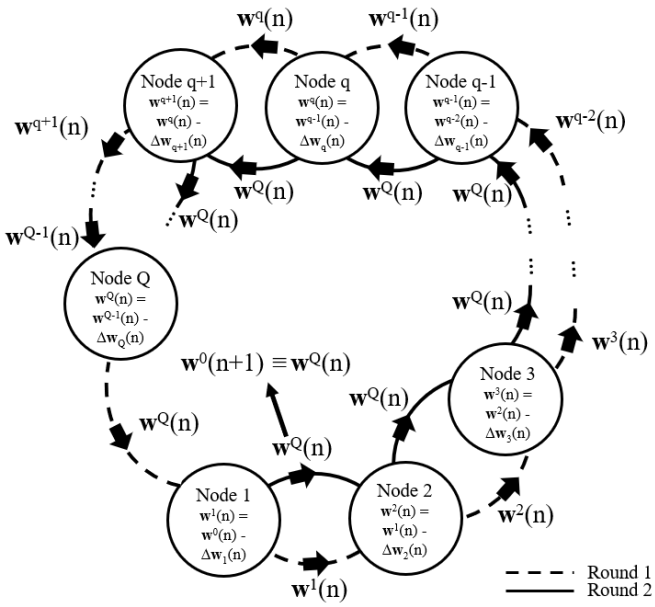


Fig. 4. A ring-topology distributed ASN with incremental learning. The algorithm is performed by two rounds within one sampling period: the first one to calculate the network state $\mathbf{w}^Q(n)$ using partial updates computed at the nodes, and the second one to disseminate $\mathbf{w}^Q(n)$ sequentially among the nodes ($\mathbf{w}(n) = \mathbf{w}^Q(n)$, $\forall q \in \{1, \ldots, Q\}$). Data transfer rounds are indicated by different type of lines.

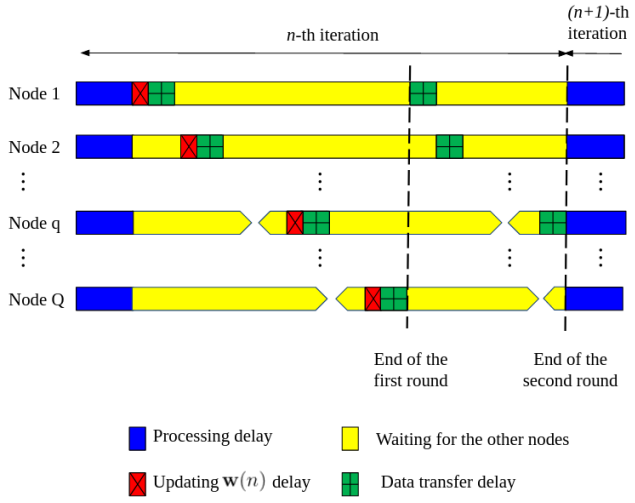


Fig. 5. Timing diagram of Algorithm 2 for a Q-node ASN including the processes carried out for each node at each sample iteration.

of the previous node, $\mathbf{w}^{q-1}(n)$, to perform its updating; green shows the data transfer delay necessary for the diffusion of $\mathbf{w}(n)$ throughout the network; and yellow denotes the period of time when the node is idle, waiting for the other nodes to finish their respective operations. Since a homogeneous ASN has been considered, all of the nodes have the same characteristics and, consequently, the time to perform each operation is the same independently of the node. Note that the total processing time of the centralized method relies only on the time the algorithm needs to process local data. In contrast, in the distributed version, it also includes the time required to update $\mathbf{w}^q(n)$ as well as to deliver this information among the nodes. It should be noted that the distributed algorithm saves computing time due to the parallel processing of each $\boldsymbol{\Delta}\mathbf{w}_q(n)$ at each node. Nevertheless, the total processing delay of the whole network for each iteration must be less than the sampling period. This condition is required in practice to run the proposed distributed algorithm and it guarantees the same performance as the centralized counterpart system.

Another important aspect that should be guaranteed is the causality of the system [47], [48]. In this regard, the following condition must be fulfilled. The minimum delay of the propagation paths between the primary source and the virtual sensors must be greater than the sum of the total processing time, the maximum delay of the acoustic paths linking the actuators to the monitoring sensors, and the maximum delay of the acoustic paths from the reference sensor to the primary source. This causality constraint can be relaxed when a harmonic excitation is considered, but it is important in broadband noise control. Since we consider ANC applications inside enclosures, where the wavelength is relatively large in comparison with the physical dimensions of the system, the causality condition is fulfilled by carefully choosing the distances among the noise source, the actuators, and the sensors. Although this (delay) causality condition is not fulfilled for all monitoring and virtual points in some setups, such as the one proposed in the next section, the (causal) observation functions obtained are accurate enough. It should be noted that propagation occurs inside an enclosure (in contrast to free propagation), the sensors are relatively close, and the observation functions are computed using multichannel measurements. Thus, reflections provide high correlation values between the monitoring and virtual signals within the working frequency band for most points. In any case if this condition is not met, it is possible to delay the error signals obtained from the virtual control points at each node in practical scenarios [49] or increase the sampling rate. When these requirements are fulfilled, assuming a network of synchronized nodes, the proposed distributed algorithm can achieve the same performance as the centralized version. Under the considered assumptions, the stability and convergence properties of the proposed distributed algorithm are identical to the centralized one [31], [50].

## III. Simulation Results

This section presents the performance of the proposed RM-DMEFxLMS algorithm compared to the RM-MEFxLMS and the MEFxLMS algorithms over a distributed ANC headrest system. To this end, an acoustic simulation environment has been developed using the room impulse response (RIR) measurements of a setup with two ANC headrest systems. Each headrest system is composed of a car seat and two control nodes. Each node is equipped with one loudspeaker and two exclusive monitoring microphones and controls the noise at all selected virtual positions. This setup of transducers attempts to emulate a practical ANC headrest application, where the creation of local quiet zones at the listener's ears is intended, e.g., within a cabin of an automobile or public

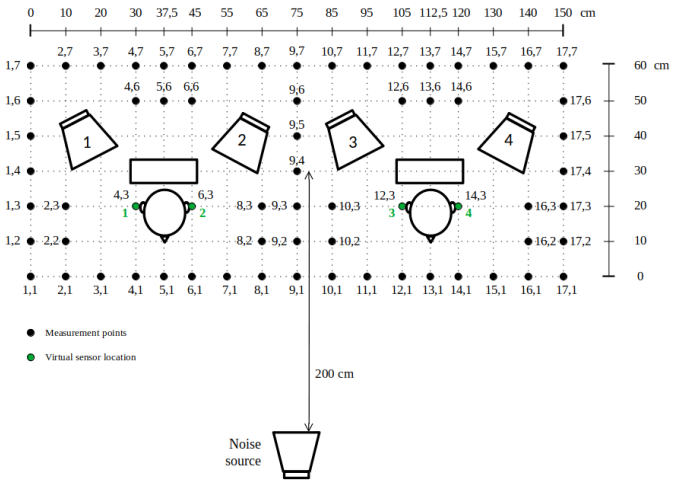


Fig. 6. Distributed ANC headrest system composed of two ANC headrest systems.

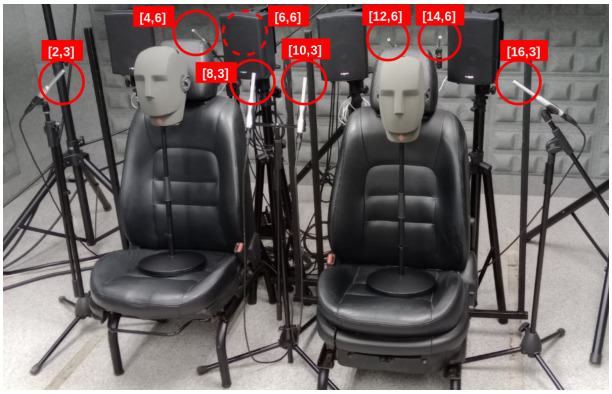


Fig. 7. Illustration of the experimental setup for measuring the acoustic channels at the specified monitoring points within the listening room.

transport. All the nodes are emulated over the same processor, which runs the distributed processing and implements the communication model performing a ring topology network. The four nodes follow an incremental learning strategy with no communication constraints (ideal communications) and perfect synchronization. For simplicity, we assume that each node has local access to the reference signal to be used directly by the algorithms. Two dummy heads seated in the chairs are used in the measurements to emulate real listeners.

With the aim of studying the effect of using the RM technique in practical environments, 67 measurement points numbered as shown in Fig. 6 were chosen as allowed locations of the monitoring microphones. Thus, a total of 335 acoustic channels were measured in a listening room of 9.36 meters long, 4.78 meters wide, and 2.63 meters high (with a reverberation time, RT60, of 0.2 seconds), located at the Audio Processing Laboratory of the Institute of Telecommunications and Multimedia Applications (iTEAM), as depicted in Fig.7. These acoustic channels were modeled as FIR filters of $M$=768 coefficients at a sampling rate of 2 kHz (which is usually high enough for ANC applications). Each pair of measurement points was 10 cm apart, except the points close to the dummy heads where the separation was 7.5 cm, as illustrated by Fig. 6.

The loudspeakers were placed adjacent to the car seats in the rear of the headrests, with a separation of 40 cm between the loudspeakers of each headrest system. The virtual microphones were placed 4.5 cm away from the dummy head ears at $[4, 3]$ and $[6, 3]$ positions for Headrest system 1, and at $[12, 3]$ and $[14, 3]$ positions for Headrest system 2, respectively (see Fig. 6). The locations of the monitoring microphones have significant impact on the calculation of the observation filters, as shown in Section III-A. The disturbance signal was rendered by a loudspeaker placed in front of the chairs, 200 cm away from the headrests. The considered disturbance signal is a zero-mean Gaussian white noise band-limited to 1 kHz with a sound pressure level of 91.1 dBSPL. The adaptive filter length was of $L$=150 coefficients. The step-size parameter for each configuration and adaptive algorithm was set as the highest value that ensured the algorithm stability. All of the microphones and loudspeakers were located at a height of 113.5 cm.

In order to evaluate the performance of the algorithms, we define the Noise Reduction (NR) at the $l$-th sensor (either virtual or monitoring), $\mathrm{NR}_l(n)$, as the ratio in dB between the estimated error powers with and without the active noise control, which is given by:

$$\mathrm{NR}_l(n) = 10 \cdot log_{10}\left[\frac{P_{e_l}(n)}{P_{d_l}(n)}\right], \tag{15}$$

where $P_{d_l}(n)$ is the power of the signal picked up at the $l$-th sensor when the ANC system is inactive and $P_{e_l}(n)$ is the error signal power measured at the $l$-th sensor when the ANC system is working. These powers were estimated by applying an exponential windowing to the instantaneous signal power. In summary, we have compared the algorithms by calculating their NR learning curves and comparing: their final values (final NR), their tendency or monotony (stability), and the shapes of these curves (convergence rate). In addition, a comparison between the presented algorithms in terms of multiplications per iteration (computational complexity) and data transfer (communication requirements) is also presented.

### A. Calculation of the observation filters

In the identification stage prior to control, the observation functions are usually modelled as $P$-coefficients FIR filters. $P$ is chosen as the lower number of coefficients to ensure accurate modelling. In addition, practical cases require including a regularization factor $\beta$ on the calculation of the observation filters to improve its robustness [18]. However, higher values of $\beta$ can result in a poor estimation of the signals at the virtual positions. Therefore, a trade-off between accuracy and robustness in the estimation as a result of a proper selection of $P$ and $\beta$ parameters needs to be considered.

Moreover, as previously commented, the ability of the observation functions to properly model the signal at the virtual points also depends on the location of the monitoring microphones. Because of this, it is convenient to present an experimental study to estimate the potential accuracy of the

remote microphone technique given the configuration considered at the beginning of Section III. Taking into account the measurements points depicted in Fig. 6, a suitable combination of positions for placing the monitoring microphones was selected to minimize the error provided by the observation functions, which are calculated following the guidelines presented in Appendix A. The study provides the best monitoring microphone configuration, which leads to the minimum Mean Squared Error between the estimated and the actual noise signals at the virtual points (MSE defined by (18) in Appendix A). To this end, some assumptions have been considered that simplify the search. Each configuration has been defined by eight monitoring microphone positions where the first four positions are physically close to Headrest system 1 and are hereby assigned to the nodes belonging to Headrest system 1. Alternatively, the other four positions are near to Headrest system 2 and consequently, are linked to the nodes of that headrest system. The optimal configuration must provide a compromise between accuracy in the calculation of the observation matrix and comfortable installation of the microphones. It is worth noting that it is not feasible to place the monitoring microphones very close to the listener's ears (for each headrest system) due to the discomfort that this location may cause to the listener.

First, different combinations of $P$ and $\beta$ were considered with the aim of leading to a minimum MSE given by (18) for each microphone configuration. The regularization parameter $\beta$ was selected as the lowest one that provides good performance on the observation functions computation and a negligible bias on the filter coefficients. Fig. 8 shows an example of the MSE at the four virtual control points for different values of parameter $P$ ($\beta$=$10^{-10}$) and a configuration with eight monitoring microphones. It can be observed that the $P$ values above 400 provide the lowest MSE. From these results, a good choice of the parameter $P$ is given by $P$=512.

Taking into account the assumptions previously considered and the values of $P$ and $\beta$, the next step is to find the best location of the monitoring microphones. Of all of the considered locations of the monitoring microphones illustrated by Fig. 6, the minimum MSE was given by the following configuration: microphones $([2,3][4,6])([6,6][8,3])$ for Headrest system 1; and: microphones $([10,3][12,6])([14,6][16,3])$ for Headrest system 2. Each pair of the selected monitoring microphones were assigned exclusively to its closest node.

Having selected the values of both $P$ and $\beta$ as well as the optimal location for the monitoring microphones, we are interested in the set of monitoring microphones that minimizes the MSE of each virtual microphone. The aim is to evaluate the suitability of using all eight available monitoring microphones in the optimal positions (or only some of them) to calculate the observation functions. Table II shows the minimum MSE at each of the four virtual microphones for several combinations of the eight monitoring microphones. The microphones selected for each case were those that gave the lowest MSE within the possible combinations of the same number of microphones (e.g., among the 56 available combinations for five monitor microphones, the case with the lowest error at the virtual microphones is shown). From the results, it can be observed that the use of the eight monitor microphones provides the best MSE (although very low MSE can also be provided from combinations of three or more microphones). Thus all of the monitoring microphones were used to estimate the noise signals at the virtual points. In summary, and given the very low MSE obtained at the virtual microphones, we can consider that a good estimation of the observation functions was achieved.

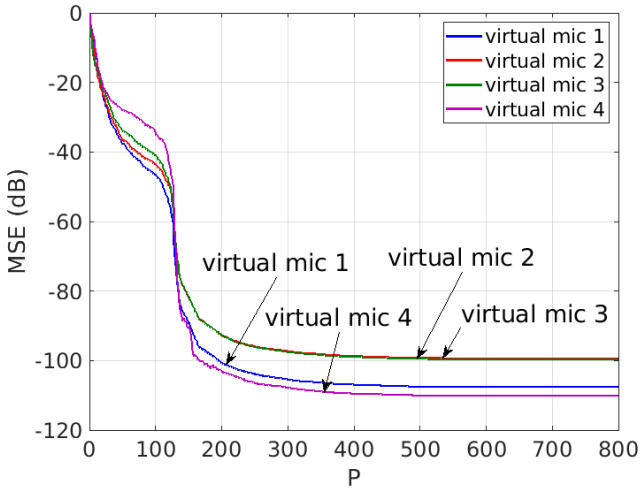


Fig. 8. MSE (dB) at the four virtual microphones for different values of $P$ and $\beta$=$10^{-10}$.

TABLE II
MINIMUM MSE AT THE VIRTUAL MICROPHONES CONSIDERING THE BEST LOCATION OF THE MONITORING MICROPHONES BY USING DIFFERENT COMBINATIONS OF THEM WITH $P$=512 AND $\beta$=$10^{-10}$. THE TERM $mic\ v$ REFERS TO $v$-TH VIRTUAL MICROPHONE.

| **Number of monitoring microphones** | **MSE (dB)** | | | |
|---|---|---|---|---|
| | $mic\ 1$ | $mic\ 2$ | $mic\ 3$ | $mic\ 4$ |
| 8 | -102.0 | -99.7 | -98.5 | -110.5 |
| 7 | -103.8 | -98.2 | -97.4 | -108.6 |
| 6 | -102.4 | -96.1 | -95.5 | -105.6 |
| 5 | -98.1 | -90.9 | -92.2 | -100.9 |
| 4 | -90.2 | -83.1 | -81.5 | -92.0 |
| 3 | -71.3 | -69.8 | -70.2 | -74.5 |
| 2 | -29.2 | -32.1 | -29.8 | -29.8 |
| 1 | -10.1 | -14.9 | -16.4 | -13.1 |

### *B. Performance evaluation of the RM-DMEFxLMS algorithm*

In this section, the performance of the RM-DMEFxLMS in terms of noise reduction and convergence rate is evaluated and compared with the MEFxLMS and RM-MEFxLMS algorithms. The set of eight monitoring microphones selected in Section III-A is considered. Fig. 9 illustrates the NR learning curves obtained for the centralized and distributed algorithms with different setup configurations for the two active headrest systems at each of the four virtual microphones. The first result (red line) illustrates the performance of the centralized MEFxLMS algorithm with a 1:4:8 configuration. Thus, the ANC system consists of one reference signal, four actuators, and eight monitoring microphones used as error sensors. As expected, when the active control is performed at the monitoring microphones, there is no attenuation at the virtual

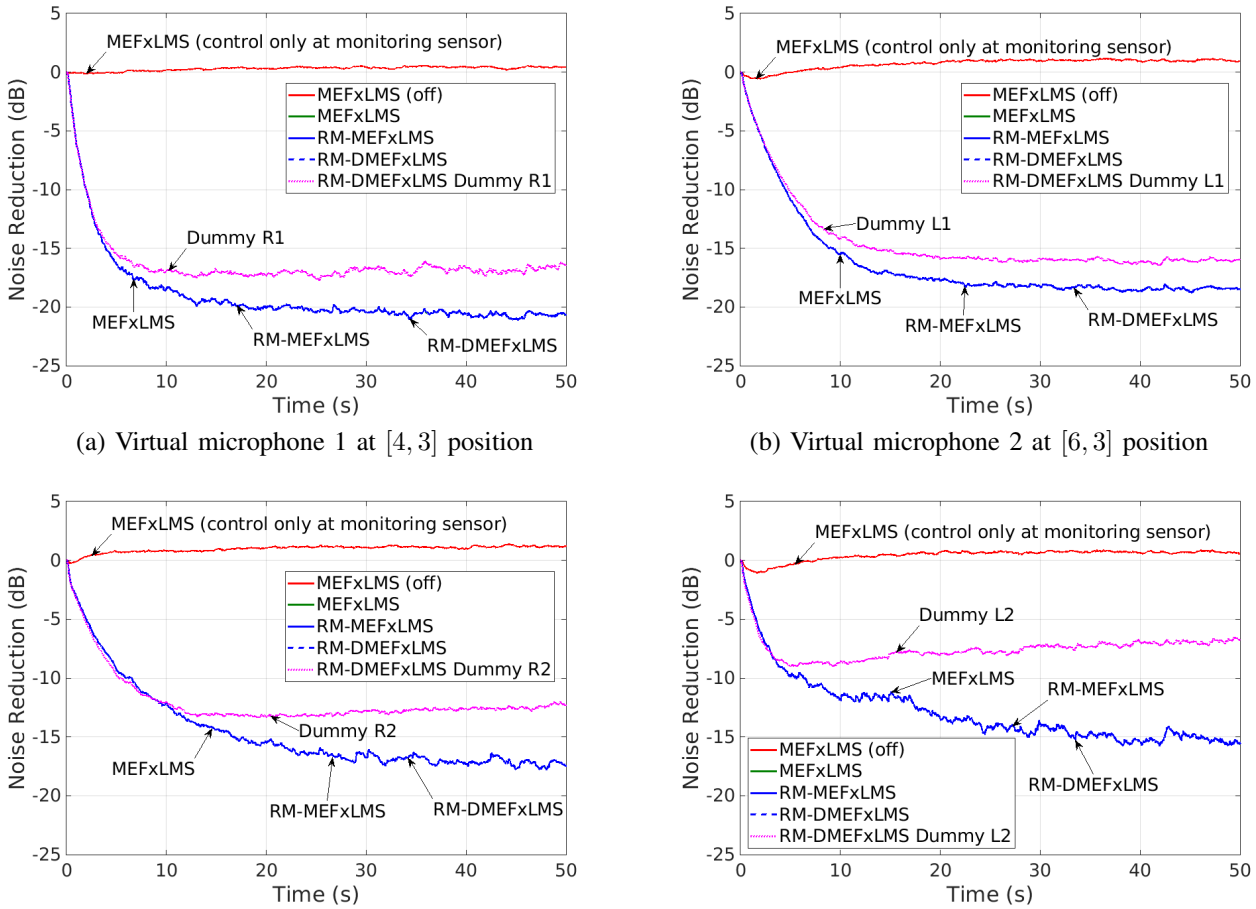


(a) Virtual microphone 1 at $[4, 3]$ position

(b) Virtual microphone 2 at $[6, 3]$ position

(c) Virtual microphone 3 at $[12, 3]$ position

(d) Virtual microphone 4 at $[14, 3]$ position

Fig. 9. Noise reduction at the virtual positions by the ANC headrest system for: MEFxLMS (controlling noise at the 8 monitoring sensors), MEFxLMS (controlling noise at the 4 virtual sensors), RM-MEFxLMS (using the remote microphone technique), and RM-DMEFxLMS (distributed version of the RM-MEFxLMS with 4 nodes). The noise reduction at the dummy head microphone closest to the corresponding virtual microphone is also showed in each figure.

sensor positions. The second result (green line) corresponds to the ideal case, in which the MEFxLMS runs in a $1{:}4{:}4$ system with four error microphones physically located at the virtual positions. The third result (blue line) is provided by the RM-MEFxLMS algorithm considering a $1{:}4{:}4$ ANC system where the four virtual sensors were used as the targets by using the RM technique. Comparing the performance of the MEFxLMS and the RM-MEFxLMS, both exhibit the same behavior at the virtual sensor positions (see Fig. 9), with NR levels higher than $15$ dB after the algorithms' convergence. These results are due to the accuracy in estimating the observation filters. However, different enclosures or set-ups of the monitoring microphones could lead to less accurate observation functions. Then higher differences in the performance between algorithms using or not using the RM technique would be observed. The fourth result (blue dashed line) shows the performance of the distributed algorithm, the RM-DMEFxLMS over an ASN comprised of four nodes with one secondary source and two error sensors at each node. As can be observed, the proposed RM-DMEFxLMS algorithm presents the same behavior as its centralized version since there are no differences between the learning curves. It shows a stable and robust behavior and provides the same noise reduction at the four virtual microphone positions. It should be noted that the distributed version of the RM technique exhibits the same performance as its centralized version when there are no communication constraints in the network. Finally, the NR measured at the dummy head microphones is also shown in Fig.9 (pink line). The NR of each dummy head microphone is represented together with the NR of its nearest virtual microphone. As expected, the NR at the dummy microphones is slightly lower than the NR at the corresponding virtual microphone.

### *C. Computational complexity and communication demands*

In this section, we evaluate the computational complexity of both centralized and distributed RM strategies in terms of multiplications per iteration at each node. The centralized version is considered a particular case of the distributed version with a single node. In parallel, the communication requirements (data transfer) of the distributed RM algorithm are also presented. To this end, we consider an ASN of $Q$ nodes. Because we assume that each node has access to the reference signal through an alternative broadcast channel, the sharing of this reference signal has not been considered

TABLE III
(1) TOTAL NUMBER OF MULTIPLICATIONS PER ALGORITHM ITERATION AT EACH NODE, MEASURED IN NUMBER OF MULTIPLICATIONS, AND, (2) COMMUNICATION REQUIREMENTS PER ALGORITHM ITERATION, MEASURED IN NUMBER OF COEFFICIENTS ( $L$: LENGTH OF THE ADAPTIVE FILTERS; $M$: LENGTH OF THE ACOUSTIC PATHS; $P$: LENGTH OF THE OBSERVATION FILTERS; $Q$: NUMBER OF NODES FOR THE DISTRIBUTED CASE; AND, $J$: NUMBER OF LOUDSPEAKERS). SEVERAL TYPICAL CASES ARE SHOWN WITH: $L$=150, $M$=768, $P$=512, $K_q$=2, $J_q$=1, AND $Q$=1, 2, 4, 8, AND 16 NODES. NOTE THAT $K=\sum_{q=1}^{Q} K_q$ AND $V=\sum_{q=1}^{Q} V_q$.

| | **Algorithms** | **Multiplications per iteration** | $Q$ **= 1** | $Q$ **= 2** | $Q$ **= 4** | $Q$ **= 8** | $Q$ **= 16** |
|---|---|---|---|---|---|---|---|
| (1) | RM-MEFxLMS | $LJ + MVJ + KVP + JV(P + M - 1) + JV(L + 1)$ | 3372 | 13188 | 52152 | 207408 | 827232 |
| (1) | RM-DMEFxLMS | $LJ_q + MVJ + K_qVP + J_qV(M + P - 1) + V(LJ + 1)$ | 3372 | 8430 | 24054 | 77334 | 272022 |
| | **Algorithm** | **Exchanged coefficients per iteration** | $Q$ **= 1** | $Q$ **= 2** | $Q$ **= 4** | $Q$ **= 8** | $Q$ **= 16** |
| (2) | RM-DMEFxLMS | $2LJ(Q-1)$ | | 600 | 3600 | 16800 | 72000 |

in the calculation of the data transfer. As can be observed from Table III, the computational complexity depends on $L$, $M$, $P$, $J$, $K$, and $V$ for both algorithms. In addition, the distributed method also depends on $J_q$ and $K_q$. On the other hand, the communication requirements only depend on $L$, $J$, and $Q$. Both implementation strategies are specified for $Q\in\{1, 2, 4, 8, 16\}$ nodes. The case $Q$=1 is omitted for the communication demands since there is no data transfer among nodes. As expected, when $Q$=1, the RM-DMEFxLMS algorithm exhibits the same computational complexity as the RM-MEFxLMS strategy. However, as $Q$ increases, Table III shows that the computational cost of the centralized algorithm is higher than the distributed approach, whose complexity at each node remains low. Note that, for the 16-node case, the reduction of the computational cost is up to 67%. With regard to the communication demands, Table III shows the data transfer needed per iteration on the whole network for the RM-DMEFxLMS. Note that, every node must transfer $LJ\times1$ adaptive coefficients to the following node using an incremental strategy. These transfers are carried out $2(Q-1)$ times within each sampling period (algorithm iteration), which means that two rounds are needed. Note that both implementation aspects, computational complexity and communication requirements, increase significantly with the number of nodes. A practical example of an ANC system working over an incremental ASN composed of 4 nodes ($Q$=4), similar to that described in [43], is considered. It uses standard audio cards working with blocks of 2048 samples ($B$=2048) and a common sampling frequency ($f_s$) of 44.1 kHz. The buffering time, defined as $B/f_s$, is then 0.0464 s. The amount of data transferred through four nodes at this buffering time is given by $2(Q-1)(LJ)\times4$ bytes. This means 393.216 kB for single-precision floating-point format (which requires 4 bytes) and a general filter length of 4096 taps ($L$=4096). Therefore, the data per second that must be transferred through four nodes is (393.216/0.0464) 8474.4 kBps (kB per second). Thus, a transfer rate at least of 8.5 MBps would be necessary to implement the DMEFxLMS algorithm over an incremental network of four nodes. Therefore, a standard Ethernet network of 1 GBps can perform the required data transfer among the nodes. In addition, the standard network capacity allows the number of nodes to be increased. However, if enough communication capacity is not available, the proposed system would not achieve the performance of the centralized system, but it could work with a slower convergence rate [31].

## IV. CONCLUSION

This work introduces a distributed version of the MEFxLMS algorithm based on the remote microphone technique for ANC. This distributed approach allows the computational cost of the equivalent centralized algorithm to be shared among acoustic nodes with lower computational capacity instead of a single high-capacity central processing unit. In addition, removing or adding secondary sources or monitoring microphones is straightforward since it only involves turning nodes on or off, leading to a more scalable and flexible system. The proposed algorithm is called RM-DMEFxLMS and reaches the same solution as the centralized algorithm over ASNs with ring topology and incremental unconstrained communication. It has been tested on a distributed ANC headrest system over an ideal ASN. In order to evaluate the performance of the RM-DMEFxLMS for ANC applications, we have carried out numerical simulations in an ASN that is comprised of two ANC headrest systems. The noise reduction obtained by the proposed approach has been compared to that achieved by its centralized version (the RM-MEFxLMS) and by the MEFxLMS algorithm (the centralized approach without the remote microphone technique). The results show that the new approach exhibits the same performance in transient and steady states as the RM-MEFxLMS, providing there are no latency or data rate constraints in the network. Furthermore, the RM-DMEFxLMS outperforms the MEFxLMS at the virtual sensor positions. In addition, a study of implementation aspects such as computational complexity and communication capabilities among the nodes in the network is also presented. We have concluded that the computational requirements of the RM-DMEFxLMS per node are lower than those of the centralized strategy. Moreover, it has been shown that the computation and data communication requirements increase with the number of nodes.

## APPENDIX A
## CALCULATION OF THE OBSERVATION FUNCTIONS

The observation functions are usually modeled as FIR filters of $P$ coefficients that we refer to as the vector $\mathbf{o}_{kv}$. The relationship between the noise signal picked up at the physical microphones placed at the virtual sensor positions and at all

of the monitoring sensors can be expressed in matrix form as

$$\begin{bmatrix} \tilde{d}_1(n) \\ \tilde{d}_2(n) \\ \vdots \\ \tilde{d}_V(n) \end{bmatrix} = \begin{bmatrix} \mathbf{o}_{11}^T & \mathbf{o}_{21}^T & \cdots & \mathbf{o}_{K1}^T \\ \mathbf{o}_{12}^T & \mathbf{o}_{22}^T & \cdots & \mathbf{o}_{K2}^T \\ \vdots & \ddots & & \vdots \\ \mathbf{o}_{1V}^T & \mathbf{o}_{2V}^T & \cdots & \mathbf{o}_{KV}^T \end{bmatrix} \begin{bmatrix} \mathbf{d}_{\mathbf{m},1}(n) \\ \mathbf{d}_{\mathbf{m},2}(n) \\ \vdots \\ \mathbf{d}_{\mathbf{m},K}(n) \end{bmatrix}, \quad (16)$$

which can be compacted as

$$\tilde{\mathbf{d}}(n) = [\mathbf{O}_1 \ \mathbf{O}_2 \ \ldots \ \mathbf{O}_K]\mathbf{d}_{\mathbf{m}}(n) = \mathbf{O}\mathbf{d}_{\mathbf{m}}(n), \quad (17)$$

where $\tilde{\mathbf{d}}(n)$ is a $[V\times 1]$ vector with the last sample of the estimated noise signals picked up at each of the $V$ virtual sensor positions when a physical microphone is located and $\mathbf{d}_{\mathbf{m}}(n)$ is a $[PK\times 1]$ vector, which concatenates the $K$ vectors composed by the last $P$ samples of the signals at each monitoring sensor. $\mathbf{O}$ is a matrix of size $[V\times PK]$ that holds all of the observation filters, which link all of the monitoring sensors to all of the virtual sensors. Moreover, $\mathbf{O}_k$ is a $[V\times P]$ matrix comprised of the observation filters linking the $k$-th monitoring sensor to all of the virtual sensors, $\mathbf{O}_k=[\mathbf{o}_{k1} \ \mathbf{o}_{k2} \ \ldots \ \mathbf{o}_{kV}]^T$.

The observation filters are calculated by minimizing the mean square error (MSE) between the signals picked up at the monitoring and at the virtual sensors. Thus, matrix $\mathbf{O}$ minimizes the following cost function:

$$\mathrm{MSE} = \mathrm{E}\{(\mathbf{d}(\mathrm{n})-\tilde{\mathbf{d}}(\mathrm{n}))^{\mathrm{T}}(\mathbf{d}(\mathrm{n})-\tilde{\mathbf{d}}(\mathrm{n}))\}. \quad (18)$$

The solution of the above problem is given by $\mathbf{O}_{opt}=[\mathbf{R}_{\mathbf{mm}}^{-1}\mathbf{R}_{\mathbf{mv}}]^T$, where $\mathbf{R}_{\mathbf{mm}}=\mathrm{E}\{\mathbf{d}_{\mathbf{m}}(\mathrm{n})\mathbf{d}_{\mathbf{m}}^{\mathrm{T}}(\mathrm{n})\}$ is a matrix of size $[PK\times PK]$ and $\mathbf{R}_{\mathbf{mv}}=\mathrm{E}\{\mathbf{d}_{\mathbf{m}}(\mathrm{n})\mathbf{d}^{\mathrm{T}}(\mathrm{n})\}$ is a matrix of size $[PK\times V]$. It should be noted that, if $\mathbf{d}_{\mathbf{m}}(n)$ and $\mathbf{d}(n)$ are measured by exciting the system with white noise, the calculation of the matrices $\mathbf{R}_{\mathbf{mm}}$ and $\mathbf{R}_{\mathbf{mv}}$ would be equivalent to the calculation of these matrices from the knowledge of the primary paths between the noise source and the monitoring and virtual sensors. Thus, $\mathbf{R}_{\mathbf{mm}}$ could be estimated as:

$$\mathbf{R}_{\mathbf{mm}} = \begin{bmatrix} \mathbf{R}_{\mathbf{mm}_{11}} & \mathbf{R}_{\mathbf{mm}_{12}} & \cdots & \mathbf{R}_{\mathbf{mm}_{1\mathrm{K}}} \\ \mathbf{R}_{\mathbf{mm}_{21}} & \mathbf{R}_{\mathbf{mm}_{22}} & \cdots & \mathbf{R}_{\mathbf{mm}_{2\mathrm{K}}} \\ \vdots & \ddots & & \vdots \\ \mathbf{R}_{\mathbf{mm}_{\mathrm{K}1}} & \mathbf{R}_{\mathbf{mm}_{\mathrm{K}2}} & \cdots & \mathbf{R}_{\mathbf{mm}_{\mathrm{KK}}} \end{bmatrix}, \quad (19)$$

with $\mathbf{R}_{\mathbf{mm}_{\mathrm{zk}}}$ being a matrix of size $[P\times P]$ defined as

$$\mathbf{R}_{\mathbf{mm}_{zk}} = \begin{bmatrix} p_{\mathbf{m},zk}(0) & p_{\mathbf{m},zk}(1) & \cdots & p_{\mathbf{m},zk}(P-1) \\ p_{\mathbf{m},zk}(-1) & p_{\mathbf{m},zk}(0) & \cdots & p_{\mathbf{m},zk}(P-2) \\ \vdots & \ddots & & \vdots \\ p_{\mathbf{m},zk}(-P+1) & p_{\mathbf{m},zk}(-P+2) & \cdots & p_{\mathbf{m},zk}(0) \end{bmatrix}, \quad (20)$$

with $p_{\mathbf{m},zk}(n)=p_{\mathbf{m},z}(n)*p_{\mathbf{m},k}(-n)$, where $p_{\mathbf{m},l}(n)$ is the impulse response of the acoustic channel between the noise source and the $l$-th monitoring sensor. Similarly, the $[PK\times V]$ matrix $\mathbf{R}_{\mathbf{mv}}$ could be estimated as:

$$\mathbf{R}_{\mathbf{mv}} = \begin{bmatrix} \mathbf{R}_{\mathbf{mv}_{11}} & \mathbf{R}_{\mathbf{mv}_{12}} & \cdots & \mathbf{R}_{\mathbf{mv}_{1\mathrm{V}}} \\ \mathbf{R}_{\mathbf{mv}_{21}} & \mathbf{R}_{\mathbf{mv}_{22}} & \cdots & \mathbf{R}_{\mathbf{mv}_{2\mathrm{V}}} \\ \vdots & \ddots & & \vdots \\ \mathbf{R}_{\mathbf{mv}_{\mathrm{K}1}} & \mathbf{R}_{\mathbf{mv}_{\mathrm{K}2}} & \cdots & \mathbf{R}_{\mathbf{mv}_{\mathrm{KV}}} \end{bmatrix}, \quad (21)$$

with $\mathbf{R}_{\mathbf{mv}_{\mathrm{kv}}}$ being a matrix of size $[P\times 1]$ defined as

$$\mathbf{R}_{\mathbf{mv}_{\mathrm{kv}}} = \begin{bmatrix} p_{kv}(0) \\ p_{kv}(-1) \\ \vdots \\ p_{kv}(-P+1) \end{bmatrix}, \quad (22)$$

with $p_{kv}(n)=p_{\mathbf{m},k}(n)*p_v(-n)$, where $p_v(n)$ is the impulse response of the acoustic channel between the noise source and the $v$-th virtual sensor.

## REFERENCES


[1] B. Rafaely, S. J. Elliot, and J. Garcia-Bonito, "Broadband performance of an active headrest," *The Journal of the Acoustical Society of America*, vol. 106, no. 2, pp. 787–793, 1999.

[2] M. Pawelczyk, "Adaptive noise control algorithms for active headrest system," *Control Engineering Practice*, vol. 12, no. 9, pp. 1101–1112, Sep. 2004.

[3] J. Cheer and S. J. Elliott, "Multichannel control systems for the attenuation of interior road noise in vehicles," *Mechanical Systems and Signal Processing*, vol. 60-61, pp. 753–769, 2015.

[4] M. Misol, C. Bloch, H. P. Monner, and M. Sinapius, "Performance of active feedforward control systems in non-ideal, synthesized diffuse sound fields," *The Journal of the Acoustical Society of America*, vol. 135, no. 4, pp. 1887–1897, 2014.

[5] D. Shi, W. S. Gan, B. Lam, R. Hasegawa, and Y. Kajikawa, "Feedforward multichannel virtual-sensing active control of noise through an aperture: Analysis on causality and sensor-actuator constraints," *The Journal of the Acoustical Society of America*, vol. 147, no. 1, pp. 32–48, 2020.

[6] Y. Song, Y. Gong, and S. M. Kuo, "A robust hybrid feedback active noise cancellation headset," *IEEE Transactions on Speech and Audio Processing*, vol. 13, no. 4, pp. 607–617, 2005.

[7] Z. Zhang, M. Wu, C. Gong, L. Yin, and J. Yang, "Adjustable structure for feedback active headrest system using the virtual microphone method," *Applied Sciences*, vol. 11 (11), 2021.

[8] H. Zhang and D. Wang, "A deep learning method to multi-channel active noise control," in *Proc. Interspeech 2021*, 2021, pp. 681–685.

[9] H. Zhang and D. Wang, "Deep ANC: A deep learning approach to active noise control," *Neural Networks*, vol. 141, pp. 1–10, 2021.

[10] H. Zhang and D. Wang, "Deep MCANC: A deep learning approach to multi-channel active noise control," *Neural Networks*, vol. 158, pp. 318–327, 2023.

[11] S. J. Elliott, P. Joseph, A. J. Bullmore, and P. A. Nelson, "Active cancellation at a point in a pure tone diffuse sound field," *Journal of Sound and Vibration*, vol. 120, no. 1, pp. 183–189, 1988.

[12] B. Lam, W. S. Gan, D. Shi, M. Nishimura, and S. J. Elliott, "Ten questions concerning active noise control in the built environment," *Building and Environment*, vol. 200, p. 107928, 2021.

[13] P. Joseph, S. J. Elliott, and P. A. Nelson, "Near field zones of quiet," *Journal of Sound and Vibration*, vol. 172, no. 5, pp. 605–627, May 1994.

[14] A. Roure and A. Albarrazin, "The remote microphone technique for active noise control," in *Proceedings of Active 99*, 1999, pp. 1233–1244.

[15] D. Moreau, B. Cazzolato, A. Zander, and C. Petersen, "A review of virtual sensing algorithms for active noise control," *Algorithms*, vol. 1, no. 2, pp. 69–99, 2008.

[16] W. Jung, S. J. Elliott, and J. Cheer, "Combining the remote microphone technique with head-tracking for local active sound control," *The Journal of the Acoustical Society of America*, vol. 142, no. 1, pp. 298–307, 2017.

[17] J. Buck, S. Jukkert, and D. Sachau, "Performance evaluation of an active headrest considering non-stationary broadband disturbances and head movement," *The Journal of the Acoustical Society of America*, vol. 143, no. 5, pp. 2571–2579, 2018.

[18] W. Jung, S. J. Elliott, and J. Cheer, "Estimation of the pressure at a listener's ears in an active headrest system using the remote microphone technique," *The Journal of the Acoustical Society of America*, vol. 143, no. 5, pp. 2858–2869, 2018.

[19] W. Jung, S. J. Elliott, and J. Cheer, "Local active control of road noise inside a vehicle," *Mechanical Systems and Signal Processing*, vol. 121, pp. 144–157, Apr. 2019.

[20] T. D. A. H. Sun, J. Zhang and P. N. Samarasinghe, "Active noise control over 3d space with remote microphone technique in the wave domain," in *Proc. IEEE Workshop on Applications of Signal Processing to Audio and Acoustics (WASPAA)*, 2021, pp. 301–305.

[21] Z. Zhang, M. Wu, L. Yin, C. Gong, J. Yang, Y. Cao, and L. Yang, "Robust parallel virtual sensing method for feedback active noise control in a headrest," *Mechanical Systems and Signal Processing*, vol. 178, Oct. 2022.
[22] T. Betlehem, W. Zhang, M. A. Poletti, and T. D. Abhayapala, "Personal sound zones: Delivering interface-free audio to multiple listeners," *IEEE Signal Processing Magazine*, vol. 32, no. 2, pp. 81–91, Mar. 2015.
[23] C. Shi, R. Xie, N. Jiang, H. Li, and Y. Kajikawa, "Selective virtual sensing technique for multi-channel feedforward active noise control systems," in *Proceedings IEEE International Conference on Acoustics, Speech and Signal Processing (ICASSP)*, 2019, pp. 8489–8493.
[24] S. J. Elliott, C. K. Lai, T. Vergez, and J. Cheer, "Robust stability and performance of local active control systems using virtual sensing," in *Proceedings 23rd International Congress on Acoustics (ICA)*, Sep. 2019, pp. 61–68.
[25] S. J. Elliott, J. Zhang, C. K. Lai, and J. Cheer, "Superposition of the uncertainties in acoustic responses and the robust design of active control systems," *The Journal of the Acoustical Society of America*, vol. 148, no. 3, pp. 1415–1424, 2020.
[26] S. J. Elliott, I. Stothers, and P. A. Nelson, "A multiple error LMS algorithm and its application to the active control of sound and vibration," *IEEE Transactions on Acoustics, Speech, and Signal Processing*, vol. 35, no. 10, pp. 1423–1434, Oct. 1987.
[27] S. J. Elliott and C. C. Boucher, "Interaction between multiple feedforward active control systems," *IEEE Transactions on Speech and Audio Processing*, vol. 2, no. 4, pp. 521–530, Oct. 1994.
[28] P. Grosdidier and M. Morari, "Interaction measures for systems under decentralized control," *Automatica*, vol. 22, no. 3, pp. 309–319, 1986.
[29] G. Zhang, J. Tao, X. Q. jun, and I. S. Burnett, "Decentralized two-channel active noise control for single frequency by shaping matrix eigenvalues," *IEEE/ACM Transactions on Audio, Speech, and Language Processing*, vol. 27, no. 1, pp. 44–52, 2019.
[30] A. P. Berkhoff, "Optimum sensor-actuator distance for decentralized acoustic control," *The Journal of the Acoustical Society of America*, vol. 110, no. 1, pp. 260–266, 2001.
[31] M. Ferrer, M. de Diego, G. Piñero, and A. Gonzalez, "Active noise control over adaptive distributed networks," *Signal Processing*, vol. 107, pp. 82–95, 2015.
[32] A. Bertrand, "Applications and trends in wireless acoustic sensor networks: A signal processing perspective," in *Proceedings 18th IEEE Symposium on Communications and Vehicular Technology. Benelux (SCVT)*, 2011, pp. 1–6.
[33] J. Segura-Garcia, S. Felici-Castell, J. J. Perez-Solano, M. Cobos, and J. M. Navarro, "Low-cost alternatives for urban noise nuisance monitoring using wireless sensor networks," *IEEE Sensors Journal*, vol. 15, no. 2, pp. 836–844, 2015.
[34] A. Alexandridis and A. Mouchtaris, "Multiple sound source location estimation in wireless acoustic sensor networks using doa estimates: the data-association problem," *IEEE/ACM Transactions on Audio, Speech, and Language Processing*, vol. 26, no. 2, pp. 342–356, Feb. 2018.
[35] M. Cobos, J. J. Perez-Solano, S. Felici-Castell, J. Segura, and J. M. Navarro, "Cumulative-sum-based localization of sound events in low-cost wireless acoustic sensor networks," *IEEE/ACM Transactions on Audio, Speech, and Language Processing*, vol. 22, no. 12, pp. 1792–1802, 2014.
[36] A. I. Koutrouvelis, T. W. Sherson, R. Heusdens, and R. C. Hendriks, "A low-cost robust distributed linearly constrained beamformer for wireless acoustic sensor networks with arbitrary topology," *IEEE/ACM Transactions on Audio, Speech, and Language Processing*, vol. 26, no. 8, pp. 1434–1448, 2018.
[37] D. Cherkassky and S. Gannot, "Blind synchronization in wireless acoustic sensor networks," *IEEE/ACM Transactions on Audio, Speech, and Language Processing*, vol. 25, no. 3, pp. 651–661, 2017.
[38] A. Bertrand and M. Moonen, "Robust distributed noise reduction in hearing aids with external acoustic sensor nodes," *EURASIP Journal on Advances in Signal Processing*, vol. 2009, 2009.
[39] C. G. Lopes and A. H. Sayed, "Incremental adaptive strategies over distributed networks," *IEEE Transactions on Signal Processing*, vol. 55, no. 8, pp. 4064–4077, 2007.
[40] C. Antoñanzas, M. Ferrer, M. de Diego, and A. Gonzalez, "Affine-projection-like algorithm for active noise control over distributed networks," in *Proceedings 9th IEEE Sensor Array and Multichannel Signal Processing Workshop (SAM)*, 2016, pp. 1–5.
[41] M. Ferrer, M. de Diego, G. Piñero, and A. Gonzalez, "Affine projection algorithm over acoustic sensor networks for active noise control," *IEEE/ACM Transactions on Audio, Speech, and Language Processing*, vol. 29, pp. 448–461, 2021.
[42] C. Antoñanzas, M. Ferrer, M. de Diego, and A. Gonzalez, "Control effort strategies for acoustically coupled distributed acoustic nodes," *Wireless Communications and Mobile Computing*, vol. 2017, 2017.
[43] C. Antoñanzas, M. Ferrer, M. de Diego, and A. Gonzalez, "Blockwise frequency domain active noise controller over distributed networks," *Applied Sciences*, vol. 6 (5), 2016.
[44] S. J. Elliott and J. Cheer, "Modeling local active sound control with remote sensors in spatially random pressure fields," *The Journal of the Acoustical Society of America*, vol. 137, no. 4, pp. 1936–1946, 2015.
[45] D. Morgan, "An analysis of multiple correlation cancellation loops with a filter in the auxiliary path," *IEEE Transactions on Acoustics, Speech, and Signal Processing*, vol. 28, no. 4, pp. 454–467, Aug. 1980.
[46] S. Haykin, *Adaptive filter theory*, 4th ed. Upper Saddle River, NJ, USA: Prentice Hall, 2002.
[47] R. A. Burdisso, "Causality analysis of feedforward-controlled systems with broadband inputs," *The Journal of the Acoustical Society of America*, vol. 94, pp. 234–242, 1993.
[48] S. J. Elliott, W. Jung, and J. Cheer, "Causality and robustness in the remote sensing of acoustic pressure, with application to local active sound control," in *Proceedings IEEE International Conference on Acoustics, Speech and Signal Processing (ICASSP)*, 2019, pp. 8484–8488.
[49] D. Treyer, S. Gaulocher, S. Germann, and E. Curiger, "Towards the implementation of the noise-cancelling office chair: algorithms and practical aspects," in *Proceedings of 23rd International Congress on Sound and Vibration*, Jul. 2016, pp. 1–8.
[50] W. Jung, S. J. Elliott, and J. Cheer, "The effect of remote microphone technique and head-tracking on local active sound control," in *Proceedings of 23rd International Congress on Sound and Vibration*, Jul. 2016, pp. 1–8.